# Percolation in nanoporous gold and the principle of universality for two-dimensional to hyperdimensional networks

G. B. Smith, A. I. Maaroof, and M. B. Cortie
*Department of Physics and Advanced Materials and Institute for Nanoscale Technology, University of Technology, Sydney, P.O. Box 123, Broadway, New South Wales 2007, Australia*

(Received 10 April 2008; revised manuscript received 5 September 2008; published 22 October 2008)

Percolation in nanoporous gold can be achieved with as little as 8% by volume of gold. Samples of nanoporous gold of various morphologies are analyzed with a combination of electrical and optical data. Growing thin films and complex multiply connected three-dimensional networks both display nonuniversal character. Growing films have two-dimensional morphology but a three-dimensional percolation threshold and nonuniversal critical coefficients, yet similar silver films percolate as expected with universal coefficients. Growing gold however regresses to two-dimensional resistive behavior between 65% to 100% gold, and this regime lies along a single power-law curve shared by the hyperdimensional networks of gold, suggesting underlying symmetry governed by diffusion-limited aggregation. Models of data imply either hyperdimensionality or major internal property changes as density shifts. The distinctive flat spectral signature found near the percolation threshold is common to all highly porous samples and is explained quantitatively in terms of effective plasmonic response. Parameters from fits of effective medium models to optical and resistivity data are in close agreement, especially at the highest porosities. They imply an effective dimension which increases continuously as porosity grows via the increased branching needed for structural integrity.

DOI: 10.1103/PhysRevB.78.165418 PACS number(s): 68.55.J−, 78.66.−w, 64.60.ah, 71.30.+h

## I. INTRODUCTION

Two component nanostructured networks with one phase metallic and the other insulating undergo a metal-insulator transition at the critical concentration of metal known as the percolation threshold. dc resistivity changes by several orders of magnitude and there are qualitative changes in optical response in the wavelength range where the dense metal would begin to reflect strongly. We will prove theoretically and demonstrate experimentally for gold that, close to percolation, far-field spectral response in the Drude region is strikingly unique, being neither metallic nor insulating in character.

The growth of metallic thin films during deposition shows a percolation transition at a critical coverage of metal. At shorter deposition times these films consist of islands of metal, and at longer times connected labyrinths of metal envelop remaining voids, which gradually close up with further deposition. The thickness ranges in these studies for metals such as gold and silver are typically below 8 to 14 nm for deposition onto room-temperature glass substrates, with some variations in critical mass and thickness according to the energetics of the deposition process.[1–5] These percolating granular films are random networks and their voids traverse the film from one side to the other. Far less experimental work has been done on more complex metal networks in which the insulating inclusions can also form complex internal networks and there is a high degree of local coordination. These are the focus of this study, with emphasis on nanoporous gold. The properties of this material near percolation are assuming technical importance as a result of the growing interest in composite nanomaterials. Emerging applications of nanoporous gold include surface-enhanced Raman scattering spectroscopy,[6,7] solar energy, thermal radiation and photonics,[8–10] capacitive biosensors,[11] supercapacitors[12] and chemical catalysis.[13,14]

Percolation theory has an extensive history,[15] which we will draw on for analysis of our data along with basic principles in phase transition theory.[16] The application of percolation theory to experimental materials has been predominantly for dc and ac electrical data on composites made from powders,[17–19] while natural structures such as porous rocks[20] and sea ice[21] have also been studied. Optical studies of metal percolation exist,[2,4,22–24] but since the far-field spectral transition is more gradual, have received much less attention. Nevertheless, percolation has a unique optical signature. Thin metal films in the early stages of growth[2–4] and nanostructured cermets[23,24] have been the main focus for the influence of percolation on optical response. Recent interest in nanoplasmonics has included fascinating data on near-field optical response in two-dimensional (2D) thin metal films close to percolation.[25,26] We focus on the unique far-field response at percolation due to plasmonic effects as part of our data analysis.

Near a critical temperature $T_c$ response functions such as conductivity or magnetic susceptibility approach criticality exponentially as $|T-T_c|^{-\gamma}$. In a two part composite, percolation theory deals with the critical behavior of material properties as a function not of temperature, but of concentration $f$ of one component, which we take to be the conductor. In lattice models $f$ represents either the fraction of occupied lattice sites or the fraction of bonds, which are conducting. In disordered composite materials, which are the subject of this paper, either continuum or random network models are needed. Then $f$ represents the volume fraction of the conducting component and the form $|f-f_c|^{-\alpha}$ describes the approach to percolation criticality at $f=f_c$. Models which map continuum "Swiss Cheese" or "random void" structures onto discrete random networks[27] can provide a link to network models to see how critical coefficients such as $\alpha$ behave in random void structures. Most of the mesoporous gold

 

samples analyzed in this paper appear to be in the form of filamental networks to begin with, but a Swiss Cheese (SC) approach remains a possibility and is thus explored optically via simulation. The relevance to our theme is that these mappings can yield critical coefficients which depart from those given by "The Principle of Universality"[16] in three dimensions, but not in two dimensions.[27] This principle states that the way in which a material's critical coefficients such as $\alpha$ and $\gamma$ vary depends only on the physical dimension.

Observed departures from universality have been seen in other percolating systems.[28,29] Explanations usually invoke internal local changes in relevant properties as $f$ varies, for example local conductance of a bond or the link between two percolating clusters in a scaling analysis of criticality.[27] An alternative is to consider that the network is hyperdimensional. Some natural structures appear to display critical hyperdimensionality[21] and, in theory, multiply connected random networks such as Bethe lattices[15] are hyperdimensional. The effective dimensionality $d$ in a finite $z$ treelike Bethe lattice is $z/2$, where $z$ represents the number of bonds emerging on average from each junction. Optical response of such networks should also be sensitive to $d$ and we explore this issue in our data analysis. As $z$ and $d$ increase, the degrees of freedom open to charge movement within a filamental network will increase. Also, as the effective dimension $d$ of structures increases, a decrease in lowest achievable $f_c$ values[15] occurs since it is easier to find a closed pathway through more complex, multiply connected networks. Morphology is thus the central issue in percolation theory and our nanoporous gold samples manifest a systematic evolution of nanostructure as production parameters are altered and porosity increases, which provides interesting new perspectives.

The unusually low $f_c$ values for a metal-void system that we will present are not a guarantee of hyperdimensionality, and other explanations of nonuniversal coefficients exist, as noted above. However the linked analysis of electrical and optical data in these random gold networks that we will now present is strongly supportive of that conclusion. To avoid confusion with the discussion of hyperdimensionality, and also to handle a dimensional critical anomaly we find in growing gold films, we will utilize the symbol $D$ to denote the spatial dimension of the structure and $d$ to denote a more general structural dimension which may differ from $D$.

Some of the porous gold structures following have $D=2$ and some $D=3$ morphologies. If a metal-insulator thin film structure has $D=2$ a vertical trace from the substrate cuts a metal-air boundary either once only, or not at all if starting under a void. For $D=3$ multiple cuts of metal-void interfaces will occur. We examine both types of gold. If the second phase is void in three-dimensional (3D) systems, only the percolating side is accessible to experiment, but we will see it is possible to approach remarkably close to the percolation threshold while maintaining structural integrity. Good stability at very high void density seems to be linked with increased branching in the network, which in turn links to effective dimensionality. In a parallel study we have found these highly porous networks to be more thermally stable than dense layers of gold.

We will commence with an outline of sample preparation and their structural, electrical, and optical characterization. Models and simulations used to understand and describe the data will be introduced when it is analyzed in Secs. IV and V. This will include a formal description of the unusual flat spectral response seen in both data and simulations at and near percolation in terms of the effective plasmonic response. Finally we will show that the parameters needed to describe optical behavior can also describe dc electrical response to a good approximation.

## II. PREPARATION AND STRUCTURE OF NANOPOROUS GOLD

It is not possible to simply study resistance $R$ *in situ* continuously during growth as we could in the thin layer case[5,12] since the process we utilize is based on etching a predeposited alloy. Second we cannot experimentally access a void-metal 3D system with subpercolation threshold $f$ values. These are only possible when the second phase is a solid insulator. Thus we need to make many separate samples to cover a range of fill factors. We note that *in situ* studies in 3D are possible with metal-insulator codeposits (called cermets), which do allow isolated particles, and are worth carrying out. Cermets were studied for percolation by Niklasson and Granqvist[23] and Cohen *et al.*[30] for different $f$ values of cobalt in $Al_2O_3$ and silver in $SiO_2$, respectively. In contrast to 2D systems these 3D structures have an intermediate regime where both phases percolate. In $Al_2O_3$:Co it is at $0.25<f_{Co}<0.7$ and in $SiO_2$: Ag it is $0.35<f_{Ag}<0.65$, but the sharpest rise in $R$ occurs at the lower $f$ values. Our nanoporous gold samples can have percolation onsets at a range of metal fill factors from similar values to these cermets, down to very much lower $f_{Au}$. Our network however is not formed by direct codeposition, though the starting point is codeposition of two metals gold and aluminum to form an alloy. After removal of aluminum the final material is nanoporous gold and as an effective medium it has two components, with the insulator phase being voids.

### A. Film preparation

#### 1. Thin gold films on glass

This study relates to preparation of gold thin films with *in situ* measurement of the nucleation and growth of a gold layer through the onset of electrical conduction. The main growth stages are, with increasing deposited material, the initial nanoisland stage, the percolation region (our main focus), and the region from onset of percolation up until the film becomes dense gold. The resistance $R_f$ of Au films has been measured during deposition using two rectangular Au electrodes, thickness 50 nm, separation 6 mm, which were first deposited on the glass substrate. Electrical connections to the electrodes were made by fine Cu wires attached by clips or silver adhesive. The film was then deposited through a rectangular hole ($10\times 6$ mm$^2$) in a mask placed in front of the substrate such that the deposited film overlapped the electrodes forming a sample of area $6\times 6$ mm$^2$. In this two-probe configuration *in situ* film resistance $R_f$ was measured at 0.5 nm thickness intervals during film deposition with the plasma on, using LABVIEW software. This procedure is simi-

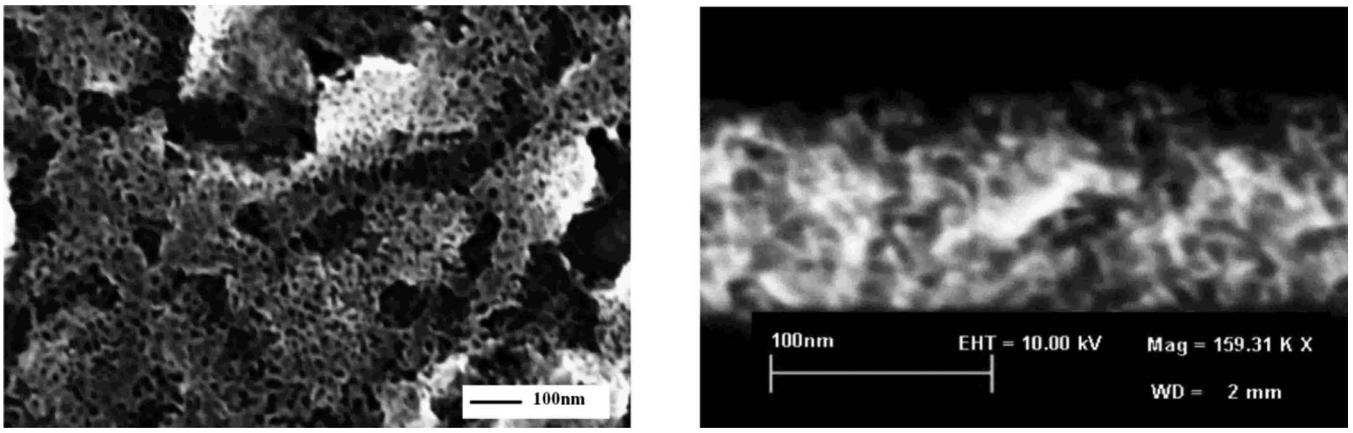


FIG. 1. Image of a nanoporous gold film on a glass substrate, to demonstrate a 3D porous nanostructure at high magnification. The right image is a cross-section view. This sample has the highest $f$ and lowest $f_c$ of those we will analyze. Its precursor alloy is deposited with the addition of ion assistance (Ref. 10).

lar to the one described by Maaroof and Evans.[5]

#### *2. Nanoporous gold films on glass*

The fabrication process of the three-dimensional nanoporous gold films is similar to that described previously.[8–10] Briefly, alloy films of $AuAl_2$ were prepared by codepositing the elements using high vacuum dc magnetron sputtering onto glass substrates. The sputtering targets of Au and Al were 99.999% pure disks (50 mm diameter), placed 150 mm away from the substrate. The base pressure was better than $\sim 10^{-6}$ Torr, while sputtering was carried out in the presence of flowing Ar at an inlet gas pressure of 8 mTorr. Most samples presented in this paper followed this procedure, but we present one which is deposited with ion assistance[10,31] as this type have highest $f_c$ values. Varying pressure enabled a wider variety of void content to be produced. To ensure good homogeneity, uniformity and crystallinity, a rotating target at 400 °C substrate temperature was used during deposition. After codepositing of $AuAl_2$ on a glass substrate, aluminum was removed from the compound by immersing the films in NaOH (0.2 M) solution. Figure 1 shows a typical high magnification image of a nanoporous gold film on a glass substrate, which displays 3D nanostructure. The right-hand image shows the cross section of the film to demonstrate it is by our definition a $D=3$ film. All the films were produced in this work at different thicknesses using a crystal monitor and the same 8 mTorr inlet gas pressure. The nanostructures of these films are shown in Figs. 2(a)–2(c). These have lower density than the film in Fig. 1 and the conventional films described in Sec. II A 1. The morphology and hence $d$ value, changes continuously with increase in thickness from 22 to 96 nm.

### B. Characterization

Scanning electron microscopy (SEM) with a Zeiss Supra55VP was used to study the nanostructure of the films. Figure 1 shows an SEM image of a nanoporous gold film with cross section clearly displaying three dimensionality. Spectral transmittance $T(\lambda)$ and reflectance $R(\lambda)$ of all nanoporous gold films were carried out using a Perkin-Elmer Lambda 950 UV/vis/NIR spectrophotometer at normal incidence over the wavelength range 300–2500 nm.

## III. PERCOLATION THRESHOLDS AND CRITICAL PARAMETERS OBSERVED IN GOLD AND SILVER THIN FILMS

Gold and silver thin films have quite distinct percolation thresholds[1,3,7,12] which can be observed as they develop during vacuum deposition. Observed $f_c=0.5$ in thin silver[1] is as predicted. Critical parameters and $f_c$ are consistent with $D=d=2$, as also found by simulation.[1] Gold behaves critically quite differently, despite going through the same growth stages and having like silver $D=2$. Figure 3 shows graphs of $R_f$ versus fractional coverage ($f$) of Au deposited on glass

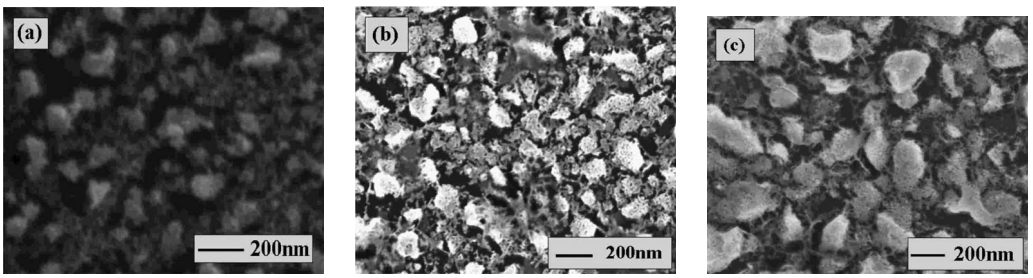


FIG. 2. SEM images of mesoporous gold film deposited at 8 mTorr with final thicknesses (a) 21.95 nm (b) 37.5 nm (c) 96.3 nm. Associated $f_{Au}$ values are derived in Sec. V. They are (a) 0.30 (b) 0.16 and (c) 0.088. Electrical properties of each follow in Sec. VI.

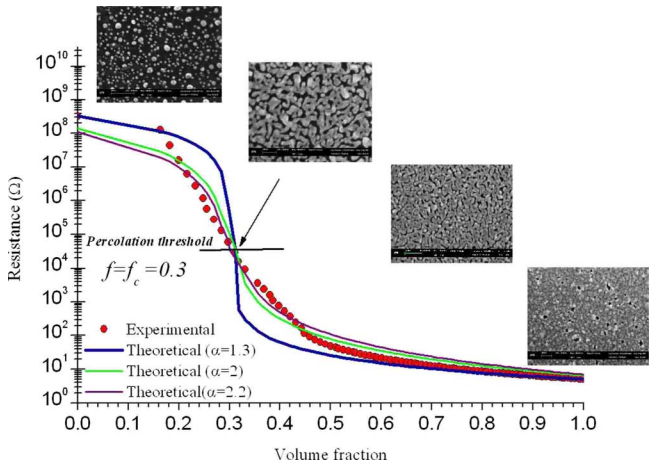


FIG. 3. (Color online) Resistance of a growing gold film on glass as a function of volume (or area) fraction $f$ of gold. Images included show characteristic morphology at each stage of gold coverage. Models for $d=2$ and $d=3$ percolation are included, along with a critical curve for $\alpha=2.2$.

obtained *in situ* for sputtered gold as the film grows. The insets show the scanning electron microscope images for four regions of nucleation and growth of the gold films. Using $t$ for equivalent thickness of dense gold deposited, actual thicknesses in the images are (i) below 3 nm ($t=0.3$ nm, $f<0.1$) (ii) 4.5 nm ($t=t_c=1.5$ nm, $f=0.33$) (iii) 5 nm to 8 nm ($t>2.5$ nm). $f$ is the ratio of equivalent thickness to actual thickness and is also given by the fractional area covered by gold. Both measurements concur quite well. In the final image (iv) the layer is almost void free and becomes so after actual thickness and $t$ coincide at $\sim 9$ nm (assuming no nanoroughness). This resistance data are consistent with a percolation threshold of $f_c=0.31\pm0.03$ as estimated using an established[5] quantitative technique based on experimental resistivity data, which also gives $f_c=0.5$ for silver. The experimental value of the percolation threshold ($f_c$) is estimated using the equation

$$R(f_c)=[R(0)R(1)]^{1/2}, \tag{1}$$

where $R(0)$ is the resistance value at $f=0$ and $R(1)$ is the metallic resistance value at $f=1$. Reference 5 provides further details on the background to this result. Image sequences as in Fig. 3 also lend support to the resulting $f_c$ values being close to $f=0.3$. Islands still appear at $f=0.25$ and continuous networks above $f=0.4$.

Plotted in Fig. 3 using this $f_c$ value are model curves of critical behavior from the standard critical relations for $R$ versus $(f-f_c)$ of Eq. (2) assuming Eq. (2a) applies out to when $f=1$. Then $A=R_{\mathrm{Au}}(1-f_c)^{\alpha_+}$ and Eq. (2a) can then also be derived from the effective medium models which will be introduced in Sec. V. However anomalies we will now discuss means this definition of $A$ may not apply to thin film gold, though we will see later it seems to work for our mesoporous samples. While different $\alpha'$s are normally required above and below percolation, we started with a common value as this works in nanoporous silver films and has been used for gold previously.[5] A plot with $\alpha_+=\alpha_-=2.2$ provides a better symmetric plot for the data than the two for $d=2$ and $d=3$ respectively but the general model of Eq. (2) spanning all $f$ does not work well for thin film gold:

$$R=A(f-f_c)^{-\alpha_+}, \quad f>f_c, \tag{2a}$$

$$R=B(f_c-f)^{\alpha_-}, \quad f<f_c. \tag{2b}$$

Curves with critical exponents expected for $D=d=2$ structures (as for silver both $\alpha=1.3$), and $d=3$ (both $\alpha=2.0$) are plotted in Fig. 3 along with the plot for $\alpha_+=\alpha_-=2.2$. Based on Eq. (2a) with $A$ dependent on $f_c$, $\alpha=2.2$ also fits poorly except maybe it is better right at criticality. Thus the general model of Eq. (2) spanning all $f$ does not work well for thin film gold. If we leave $A$ and $B$ as arbitrary parameters rather than dependent on $f_c$ and restrict exponent fitting to $R$ values within 2 orders of magnitude of $R(f_c)$ two different but low critical exponent values emerge from quite linear log–log plots. They are $\alpha_+=0.74$ and $\alpha_-=0.21$. This is anomalous with $d$ values below 2 implied along with much higher $f_c$ than the observed value of 0.31 and at odds with images. For $f>0.6$ it is interesting that the expected $\alpha=1.3$ plot works best, that is $d=2$ does apply there. Unlike silver films for which Eq. (2a) works reasonably at all $f$,[1] gold porous film morphology and hence final critical behavior seems to evolve continuously as $f$ varies. In Sec. VI we look into this in more detail where continuous evolution in morphology and associated $f_c$ is seen to be characteristic of a much wider class of porous gold. Even allowing for an evolution in morphology the critical zone data for $0.15<f<0.40$ in Fig. 3 will be shown to be different from all other nanoporous gold films in this study, which display common self-similarity at all $f$.

$f_c=0.33$ and $\alpha_+=2.0$ are expected if $d=3$. A shift from 2.0 to near 2.2 might be explained on the basis of internal local scaling related changes,[27,28] or distributions of local electrical properties in the system,[28,29] but from 1.3 to near 2.0 or 0.7 is very hard to justify along these lines. In electrical low-frequency studies of three-dimensional metal-insulator particulate composites $\alpha_+=2.0$ and $\alpha_-=0.87$ are commonly used or found.[18,19] In our $D=2$ films the $\alpha$ values and the evolution of morphology at lower $f$ may be complicated by the influence of the substrate but it is clear that expected critical coefficients are incompatible with data. Reference 19 attributes most observed shifts from universality in the electrical problem to local interface effects. Our study is confined mainly to $f>f_c$ and charge may not need to jump across interfaces in these continua even close to $f_c$. We will attribute any nonuniversality to the disordered network structure rather than interfaces. Only in the 3D Swiss Cheese model were significant shifts in exponents expected when averaging over local effects[27,28] and then only by around 0.5. Thus these various approaches do not seem to explain this gold system. It is our first example where apparently $d\neq D$ at least for $f$ close to $f_c$. These results for gold films have also been seen by others[3] and are quite distinct from those of silver. Gold clearly links up more quickly. The morphologies of Ag and Au both evolve in the fashion noted above from islands to voided conductor, but percolation at lower $f$ implies a different more open morphology at the percolation point for

gold. The eventual reversion to $d=2$ behavior as more gold is added is also indicative that $D=2$ holds at all $f$ as it is the thicker layers that would be more likely to show $D=3$ character. Just before percolation these thin layers of gold are islands and do not have three-dimensional cross sections, a claim sometimes made simply on the basis of the experimental value of $f_c$. These $f_c$ values can be explained theoretically in two ways, either average particles in a cluster near percolation have $z=6$ nearest neighbors (see Sec. IV for details), or via a "Swiss-cheese" continuum percolating system. A "Swiss-cheese" simulation for $D=2$ does predict that $f_c=0.33$.[19,32] However, universality would still require that $\alpha=1.3$, while in two dimensions mapping onto a network with correlation length scaling was predicted to give no shift in $\alpha$.[27] Thus we have to conclude that while the random overlapping void approach can explain the value of $f_c$ in growing gold films it cannot explain their departure at percolation from universality. This example may be indicative of a more general need to consider that critical dimension $d$ can differ from physical dimension $D$. Increasingly higher $d$ values cannot be ruled out in nanoporous metals and we now turn to samples of nanoporous gold for which $d>3$ is a possible explanation of their optical and electrical percolation responses.

## IV. EXPERIMENTAL AND MODELED OPTICAL AND ELECTRICAL PROPERTIES

To characterize and model the filamental mesoporous systems made by etching alloys requires a different approach to that adopted for the 2D thin films in Fig. 3. Unfortunately as already noted, we do not have a continuum of data for one critical curve, even for $f$ above $f_c$, as growth by etching means each sample has different $f$ and different structure so we cannot easily create a plot like that in Fig. 3. Simply changing metal content, which we will do, does not provide a sequence of identical morphology. Instead we will see that $f$ and $f_c$ fall in tandem for our preparation conditions, which may be the basis of stability at high void content in 3D metal-void systems. Ideally to explore critical percolation parameters, we would like to make a set of samples with the same $f_c$ value but different $f$. However every change in $f$ with the same vacuum deposition conditions leads in practice to a different morphology, with our etching process involving much gold atom movement.[8–10] A universal curve that follows may mean that in random self-supporting systems in three dimensions, self-assembled porous structures at low $f$ always do this, but further work is needed to rule out such growth along the same critical curve. The approach we adopt is to model optical and electrical data separately to estimate $f$ and $f_c$ and compare key parameters for consistency. We start however with an extended study of how percolation manifests itself in the optical domain as this not only helps in providing fairly directly an indication of how close to $f_c$ a particular sample is without modeling, but helps in assessing the merits of alternative models. In the final section an overview is provided which interestingly sheds quite new insights into the Au thin film problem raised in Sec. IV, along with further assessment of the notion that nanoporous gold approaches the critical point (even though it may not get there) consistently with $d>D$, with most $d$ values hyperdimensional.

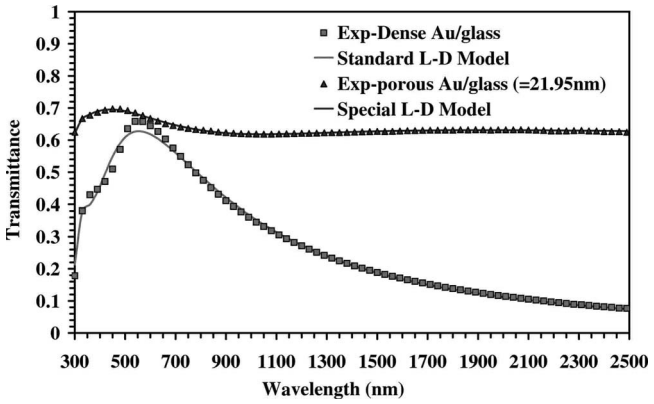


FIG. 4. Flat spectral transmittance of a mesoporous gold film near the percolation threshold compared with that of a dense gold layer. A Lorentz-Drude (LD) model is seen to fit both layers and the associated dielectric constants for the porous layer were also fitted accurately with an effective medium model.

### A. Percolation impacts on spectral response

Metal-insulator transitions in principle mean a shift from reflecting to transmitting dominance at wavelengths that do not include interband transitions of either species. However as $f$ varies through a percolation transition the plasmonic response of the metal comes into play in interesting ways. It occurs at long enough wavelengths that the real part $\varepsilon_1$ of the complex dielectric constant $\varepsilon=\varepsilon_1+i\varepsilon_2$ is negative. It is responsible for the unique optical characteristics for $f$ very close to $f_c$ can lead to spectral structure when the metal is isolated due to particle surface plasmon resonances and, once the metal is percolating, void-related resonant effects may be possible. The last two have received some recent attention for the types of thin films discussed in Sec. III (Refs. 25 and 26) but are not an issue for our $D=3$, Au filamental structures where the gold is always percolating and where strong void-related resonances do not appear to be present according to the smooth spectral data.[8] Close to percolation a unique spectral character arises which is neither metallic or insulating in the plasmonic regime for gold as seen in the spectral transmittance plot of Fig. 4 for an example mesoporous thin film compared with a dense gold film. The zone of most interest is where dense thin gold changes from transmitting to highly reflective in the range 0.55–3 $\mu$m. Near percolation in all nanoporous gold we find if fill factors $f$ are below 0.4 then the spectra are qualitatively similar to the flat curve in Fig. 4.

Reflectance and absorptance spectra are also relatively flat, as in the absorptance plot for three nanoporous films in Fig. 5. It is flatter still in reflectance as in Fig. 4 and for other such samples.[10] This unusually flat spectral response occurs in a region where gold films normally undergo a large optical change as wavelength falls, as exemplified by the plot for a dense Au thin film in Fig. 4. The other relevant point seen in

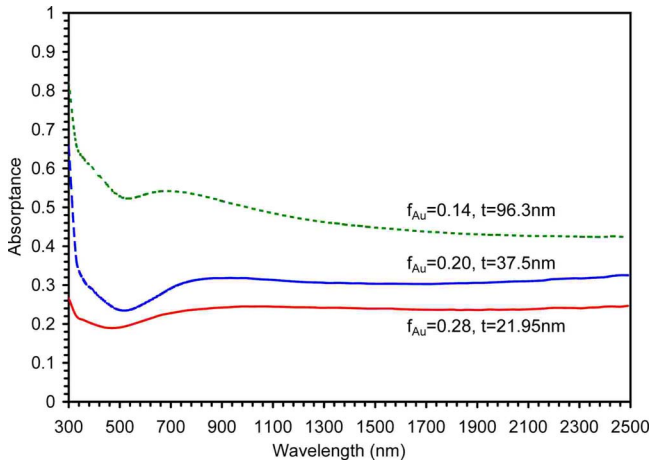


FIG. 5. (Color online) Spectral absorptance of mesoporous gold films all close to different low $f_c$ percolation thresholds.

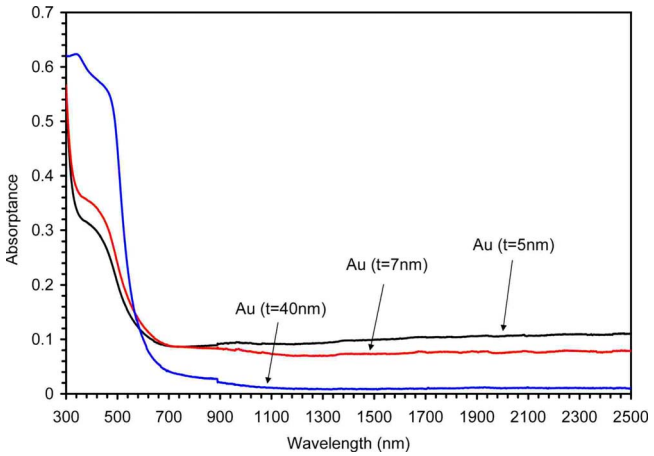


FIG. 6. (Color online) Spectral absorptance of two vacuum grown porous gold films in the percolating regime near $f_c=0.3$ compared to a continuous layer. The 5 nm layer is just percolating. Absorptance drops at larger coverage due to high reflection.

Fig. 4 is that the spectral features due to the lowest energy interband transition in gold, which is at 3.5 eV, are largely unaffected in location as void content increases. There is thus a wide band near percolation where effective refractive index is nearly constant.

Why is this? It follows primarily because nanoporous thin films when percolating behave as if they are homogeneous with an effective plasma frequency $\omega_P^*$ which is much less than the $\omega_P$ value in dense gold. The quantitative link between $\omega_P^*$ and $\omega_P$ has been derived previously[8,9] both in the general Bergman-Milton (BM) formalism and in terms of the quasistatic effective medium approach due to Bruggeman.[33] The result in the Bruggeman approximation is that

$$\omega_P^{*2} = \omega_P^2 \frac{(f - f_c)}{(1 - f_c)}. \tag{3}$$

Effective plasma frequency thus falls to low values as $f$ approaches $f_c$ and of course vanishes once the system ceases to percolate. Direct measurement of $\omega_P^*$ gives an independent and useful measure of $f$ using the BM formalism.[9] The fall is due to a combination of the drop in average free electron density, and a rise in carrier effective mass $m^*$ in the complex network as $f$ falls toward $f_c$.[8,9] An effective Drude response results, such that over the near-infrared (NIR) the plasmonic transition has not yet occurred or is weak. This idea is supported by the LD model fit in Fig. 4. A large energy gap opens up between the interband term and any weak plasmonic effects. Consequently the effective dielectric constant $\varepsilon^*$ of the porous network is almost constant for $\lambda > 1.2$ $\mu$m, as seen in the data in Figs. 4 and 5. Thermal emittance data[8] indicate reflectance does not rise much more, at even longer wavelengths. We suggest the onset of the ability to fit an effective Drude model to optical data should be a good guide to pinpointing critical percolation. Equation (2) is expected to take on a different form involving critical exponents for $f$ quite close to $f_c$ if for example we used the phenomenological effective medium models proposed by McLachlan and co-workers and used by Cai *et al.*[17–19] in place of the Bruggemann model. To explore this we would need a range of samples with fixed $f_c$ which we do not have, so it will not be addressed in this paper. It will be presented as an interesting and direct approach to extracting critical coefficients from optical data, which does not seem to have been attempted as yet.

This simple argument based on plasma frequency cannot fully explain the weak spectral structure around 850–950 nm, while the strength of absorptance in all Fig. 5 samples requires additional comment as it is higher than the simple argument above implies. It is mainly due to the elevated relaxation frequencies in these filamental nanostructures[8] arising from surface scattering of carriers. These impact on the Drude response in the flat zone and are an order of magnitude higher than that in dense gold films (0.80 to 1.0 eV versus 0.09eV). They are also the main limit on the rise in reflectance at even longer wavelengths. This flat spectral response in the Drude region appears to be a universal signature of proximity to percolation in nanostructured metal films. All three films in Fig. 2 are each close to the percolation threshold on this criteria indicating that $f_c$ is dropping as $f$ falls. The flat NIR response is also apparent in Fig. 6 for the thin gold discussed in Sec. IV, and shows up in simulation studies.

## V. QUASISTATIC MODELS AND SIMULATION OF SPECTRAL RESPONSE

We have adopted two approaches to modeling. The first is to fit our data with a suitable quasistatic effective medium model of optical response. This provides estimates of volume fraction $f$ and the threshold $f_c$. Phenomenological extensions for the region where $f$ is very close to $f_c$ have been applied to ac and dc data[17,18] though this approach has not to our knowledge been applied to date in the optical domain. Since the value of $f_c$ shifts as $f$ falls in our nanoporous gold, it is likely that critical exponents will also change. As we are thus unable to measure or fit exponents directly, we will use the standard symmetric Bruggeman model, which does give excellent fits to our spectral data. We will test its predictions in

the next section for self-consistency with equivalent effective medium models of resistivity to add further support to the merits of this simple approximation. When it works best, in terms of the gap $(f-f_c)$, will however turn out to be surprising. Our second approach is to simulate the extinction response in two complementary ways; with of a continuous gold layer containing randomly placed voids, and with an aggregation of intersecting or sintering gold particles. These have quite different critical thresholds and we examine their suitability to both two- and three-dimensional structures. The former is the SC approach and in the two-dimensional case it may apply to the growing gold films discussed in Sec. IV, when its voids cross the layer.

In the optical domain the simplest form of the Bruggeman model for effective dielectric constant $\varepsilon^*$ is expressed in terms of an effective depolarization factor $L$ as

$$f_{\mathrm{Au}}\left[\frac{\varepsilon_{\mathrm{Au}}-\varepsilon^*}{\varepsilon^*+L(\varepsilon_{\mathrm{Au}}-\varepsilon^*)}\right]+(1-f_{\mathrm{Au}})\left[\frac{1-\varepsilon^*}{\varepsilon^*+L(1-\varepsilon^*)}\right]=0. \tag{4}$$

$L$ is usually linked in such models to the shape of average cells or structural units.[34,35] Percolation occurs in the model in Eq. (4) at $f=L$. However if $L$ does not equal 1/3 one expects either optical anisotropy, or must replace Eq. (4) with an average over random orientations, using a complete suite of two or three $L$ values.[2,22,36] In addition it is quite possible that the two components, Au and voids, have on average different $L$ values, which in the context of Eq. (3) means different $L$ values in the two terms say $L_1$ and $L_2$. Two thresholds at $f=L_1$ and $f=L_2$ follow with three percolation zones as for the cermets. The important feature in this work is the relevance of Eq. (4) and some of its variants to percolation. *For spherical symmetry* $f_c=L=0.33$, but our dilemma is that we clearly have samples which are percolating at much lower $f$ values than 0.33 so we cannot rule out anisotropy. The images in Fig. 2 could indicate three-dimensional anisotropy with in-plane isotropy. These are the ones with low $f_c$. The porous films like those in Fig. 1 however do appear to be completely isotopic and ellipsometry confirms this. Best fits to these type of films with Eq. (3) do in fact give $L\sim 1/3$ and hence imply for these structures that $f_c=0.33$. It is interesting that these have the same critical threshold as standard gold thin films, despite their quite different structure.

Equation (4) gives excellent fits to complete spectral data,[9,10] especially in the critical NIR zone with $f$ and $L$ plus layer thickness $t$ as the only adjustable parameters. Good fits are found for all the low $f$ films at normal incidence where the field is in the plane. Resistivity is also measured in the plane of the films. Thus we will put the possible complexities of anisotropy aside for thus study, assume in-plane anisotropy and use the $f$ and $L$ values predicted by Eq. (4). An additional check on this approach comes from the ability to also optically fit effective layer thickness $t$ using this basic model, since $t$ has been measured independently on some samples using SEM cross sections as shown in Fig. 1(b). Estimates of mass of gold deposited during deposition plus the thickness value also give an indication of void content, though this is a lower limit only as some gold is lost on etching. Cell shapes which are oblate would be consistent with the assumption of in-plane isotropy, and this approach is backed up in three ways; by the quality of spectral fits to normal incidence data, the consistency we will demonstrate between parameters used in optical and electrical data fitting, and actual images of structure as in Figs. 1 and 2. The implication of this approach for percolation in low $f$ Au-void networks is that there is only one in-plane threshold. The alternate to the Bruggeman fitting is modeling with a basic Lorentz-Drude model of $\varepsilon^*$. This also works well, as in the example shown in Fig. 4 and elsewhere.[9,10,26] It also supports the idea of an effective homogeneous plasma system.[8] The simulation study adds further insights to these results, but is limited in scope since we only work with spherical holes or particles in setting up the nanostructures.

A simulation of how percolation in mesoporous gold impacts on optical response has been reported[32] using the discrete dipole approximation[37,38] and starting with a dense 3D layer which is then part-filled with randomly placed voids.[39] This is the Swiss Cheese model and it was found for spherical voids that $f_c=0.33$. We have since studied its counterpart formed from intersecting spheres. The extinction in all of these simulations is dominated by absorption. The structure made by adding particles which can intersect does not appear to percolate optically until $f\sim 0.6$. In porous gold we find no experimental evidence of such high $f_c$ values and thus can eliminate the intersecting particle model. The Swiss Cheese model in contrast could apply to both growing thin film data and the samples of the type in Fig. 1 which both have $f_c$ near 0.33. However neither a Swiss Cheese nor particle aggregation model as set up here is able to describe the nanoporous samples with $f$ and $f_c$ below 0.3. This is due to limiting this simulation study to spheres and hence optically isotropic systems. A need to introduce lower $L$ values for the randomly placed voids and maybe to make them oblate to simulate what we see in low $f_c$ systems is implied by this result.

Spectral absorptance data in Fig. 5 for the nanoporous gold films made by etching are qualitatively different to that in Fig. 6 for the thin two-dimensional gold layers made directly by vacuum deposition. For these layers at wavelengths beyond 900 nm, percolating films show falling transmittance and in nonpercolating films it rises. In Fig. 6 it can be seen that the 5 nm thick layer is above but very close to percolation. The 7 nm layer is well above the percolation threshold. We estimate the critical thickness to be at 4.5 nm for our sputter deposition conditions. This value is supported by a different approach to quantitatively estimate the percolation point using a formula based on resistance values over time.[3] For all of the porous layers made by etching with $f$ below 0.2, the transmittance spectral plot is exceptionally flat at NIR and longer wavelengths. This implies, as noted above, that all samples despite their differences in $f$ are close to a percolation threshold specific to each sample.

### A. Linking resistivity and optical models: the case for hyperdimensions

Considering the way gold evolves, and to link consistently with the effective medium analysis (EMA) of optical

TABLE I. Measured resistivity of mesoporous gold films as a function of fill factor and associated SEM images.

| Resistivity ($\mu\Omega$ cm) | $f$ (Percolating gold) | Sample SEM image (Figure number) |
|---|---|---|
| 1350 | 0.088 | 2(c) |
| 317 | 0.15 | 2(b) |
| 163 | 0.30 | 2(a) |
| 36.5 | 0.47 | 1 |

data, we analyzed resistivity data with both the symmetric and asymmetric dc analogs of the optical EMA. The general form is given by Eq. (5a) (Refs. 17, 18, and 40) with one phase metal and the other insulator, each with conductivities $\sigma_m$ and $\sigma_i$, respectively. It is expressed in terms of effective dimension $d=z/2$ as defined by the average branching number $z$ at each junction in a bond percolation model.[41] The symmetric EMA has both $\alpha's=1$ and is the direct dc equivalent of the Bruggeman optical model which is widely used for nanoporous materials, and its symmetric analog has also been used in the dc limit with voids as the insulator.[40] dc electrical data in Table I has been fitted to find $f_c$ for various possible critical exponents in Eq. (5a) including $\alpha=1$. The asymmetric version of Eq. (5a) has been widely used for low-frequency studies of metal-insulator composites[17–19,40] but does not seem to have been applied to highly porous percolating metals,

$$f_{\mathrm{Au}}\left[\frac{\sigma_{\mathrm{Au}}^{1/\alpha_+}-\sigma^{*1/\alpha_+}}{\sigma_{\mathrm{Au}}^{1/\alpha_+}+(d-1)\sigma^{*1/\alpha_+}}\right]+(1-f_{\mathrm{Au}})\times\left[\frac{\sigma_i^{1/\alpha_-}-\sigma^{*1/\alpha_-}}{\sigma_i^{1/\alpha_-}+(d-1)\sigma^{*1/\alpha_-}}\right]=0. \tag{5a}$$

With voids as the insulator phase $\sigma_i=0$ and we obtain for the symmetric model

$$\sigma^*=\sigma_{\mathrm{Au}}\frac{f_{\mathrm{Au}}-\frac{1}{d}}{1-\frac{1}{d}}, \tag{5b}$$

while the asymmetric models yield at $f>f_c$ and with $\sigma_i=0$,

$$\sigma^*=\sigma_{\mathrm{Au}}\left[\frac{f_{\mathrm{Au}}-\frac{1}{d}}{1-\frac{1}{d}}\right]^{\alpha_+}, \tag{5c}$$

which is in effect identical to Eq. (2a) if applicable at all $f$. $d$ is allowed to take on arbitrary values in these models[41,42] and percolation clearly occurs when $f=1/d=f_c$. Since optical spectra and dc conductivity arise from the same structure with the same critical concentration then comparing Eqs. (4) and (5) one might expect

$$f_c=L=\frac{1}{d} \tag{6}$$

This simple relation would break down if significant current transport could occur even when the metal is not quite linking up via say tunneling, a process which has been proposed in some percolation systems.[43,28,29] Discrepancies, if any, would normally be more likely if both relations become imprecise as $f$ approaches $f_c$, but we find the opposite. That is, in our data that follow, the predictions of the two simple models are most consistent and accurate when $f$ and $f_c$ are smallest, and also very close in value, while the two model predictions diverge most at the highest $f$ samples which have $f$ near 0.5 and $f_c$ near 0.3. The opposite trend as $f$ varies was expected since the basic EMA models are expected to work best at $f$ values well away from $f_c$ and to break down for $f$ close to $f_c$. We believe the most likely source of this anomaly is that our assumptions about in-plane isotropy may be less accurate in this concentration regime but future studies are needed to better understand the origins of this counterintuitive outcome.

Before the self-consistency overview and the comparison with asymmetric models, we present a table of resistivity data as a function of $f$ in Table I. The $f$ value used is based on good fitting of optical spectra with the BR model. Since all four samples shown are percolating, one approach might be to consider that these systems have a vanishingly small critical threshold and that all samples are then far from the critical zone.

A single curve for $R$ as a function of $f$ might support this idea, though such a plot could also be indicative of the way gold porous nanostructures adapt to maintain their self-supporting ability. Put simply, as $f$ increases $z$ also increases, since a higher $z$ value adds strength to the network. In other words morphology is evolving at low $f$, with a continuous change in $z$, hence in $d$ needed to maintain structural integrity. We also find indications of the evolution of morphology with falling $f$ on a closer analysis of the thin film resistivity data. Does this evolution stop at some high $f$ value once $z=4$ or $d=2$ morphology is present? Analysis of the thin film data to follow indicates that at $f$ above 0.65, $d=2$ behavior does occur and no further morphology changes arise as $f$ increases further. *This also means significant morphology change has occurred in gold films with f* below the fc where $d=3$ applied. We have combined this $d\sim 2$ segment at $f>0.65$ of thin gold film data with the data in Table I to produce the interesting plot in Fig. 7. The normal film data are clear from the closely spaced data points. The continuous curve is a best fit plot which can be reduced to a simple exponential form of Eq. (7),

$$R=5.18\left[\frac{1}{f^{2.35}}\right]. \tag{7}$$

The exponent fit has some uncertainly in the range 2.25 to 2.50. It is indicative of a universal fractal-like response probably linked to the way gold atoms diffuse and aggregate when free to move, both during etching in bulk, and on a glass surface at higher densities. It is interesting to note that the fractal dimension for random diffusion-limited aggrega-

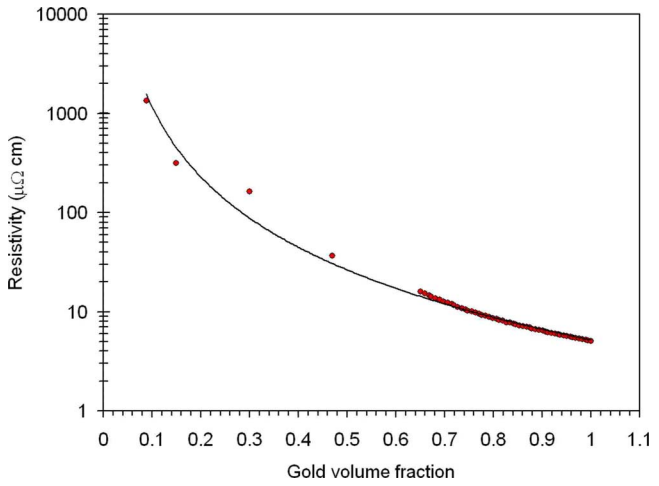


FIG. 7. (Color online) Resistivity as function of gold volume fraction $f$ for four mesoporous gold films plus a subset of normal gold films with $f>0.65$. The continuous curve is a best fit plot to indicate possible universal behavior.

tion in three dimensions is commonly stated to be 2.50. While this plot indicates that the percolation threshold itself is elusive in these porous gold structures, it is still instructive to examine these films from a hyperdimensional percolation perspective. This will also give us better insights into where all the standard gold thin film data fit into the complete picture, and also allow us to see how close to the percolation point, at which structural collapse occurs in this case, one can get as $f$ varies. Apart from estimates of $f_c$ this analysis also allows the predictions of the simple models of resistivity and optical data when fitted to our data to be tested for self-consistency.

The results of fitting Eqs. (5a) and (5b) to data to find $f_c$ and hence an estimate of effective hyperdimension $d$ and the consistency of these predictions with those of optical models are in Tables II and III. Predicted $f_c$ values are more sensitive to $\alpha$ at higher $f$ values. These tables indicate that using the symmetric EMA for optical modeling gives useful approximations to $f$ and $f_c$ especially for high $d$ value systems. Optical modeling with an asymmetric power-law EMA model is a task for the future but these tables indicate that predicted fill factors are not expected to shift much. The effective $d$ values in Table II are calculated using the averaged values of $f_c$ (labeled $\langle f_c \rangle$) from the two sets of data. The agreement between all models and optical and dc data appears surprisingly to be much better the closer $f$ gets to $f_c$. The proximity to $f_c$ is quite remarkable in the lowest $f$ samples.

TABLE II. A summary of the parameters derived from fitting optical and electrical data with $\alpha=1.0$ for the four mesoporous films using $f_c=1/L$ for optical data and $f_c=1/d$ for resistivity data.

| Gold fill factor $f$ | Critical threshold $f_c$ (Optical) | Critical threshold $f_c$ (Resistivity) | $f-\langle f_c \rangle$ | Effective $d$ $(1/\langle f_c \rangle)$ |
|---|---|---|---|---|
| 0.47 | 0.33 | 0.38 | 0.11 | 2.8 |
| 0.30 | 0.26 | 0.28 | 0.03 | 3.7 |
| 0.16 | 0.145 | 0.150 | 0.012 | 6.8 |
| 0.088 | 0.084 | 0.086 | 0.003 | 11.7 |

TABLE III. Comparison of $f_c$ values from dc data predicted by varying $\alpha_+$ in Eq. (5c) for the samples in Table II.

| Gold fill factor $f$ | $f_c(\alpha=1.0)$ | $f_c(\alpha=1.3)$ | $f_c(\alpha=2.0)$ | $f_c(\alpha=2.7)$ |
|---|---|---|---|---|
| 0.47 | 0.38 | 0.39 | 0.42 | 0.43 |
| 0.30 | 0.28 | 0.28 | 0.29 | 0.29 |
| 0.16 | 0.15 | 0.14 | 0.14 | 0.14 |
| 0.088 | 0.086 | 0.085 | 0.086 | 0.086 |

As an additional check, a series of three plots of Eq. (5b) using the $L$ and $f$ values from optical fitting, and assuming $L=1/d$ appear in Fig. 8, along with the data points from Table II. To complete the overview with another important insight, we include in this figure the complete resistivity data for growing gold films from Fig. 3, along with the two basic models appropriate to the observed $f_c$ value of 0.31 and an $f_c$ value of 0.5. The latter was expected on the grounds of the two-dimensional structure. A curve is not plotted for the sample with $f=0.47$, only the data point to avoid clutter. A curve with $f_c=0.33$ would pass just below that data point.

This figure and Fig. 7 need to be looked at together. First gold films do behave as expected at high enough $f(>0.65)$ but morphology clearly shifts at lower $f$ to yield near three-dimensional criticality in terms of an $f_c$ value near 0.33 in a random system. The observed low critical exponent is however inconsistent with this $f_c$ value. All samples whose data lies along the curve in Fig. 7 can be modeled with consistent values of $d$, $f_c$ and $\alpha$, but not the gold films (except at high $f$). The low $f$ mesoporous samples can thus be modeled successfully as high hyperdimension systems. Second, the model plots of resistivity based on the optically derived pa-

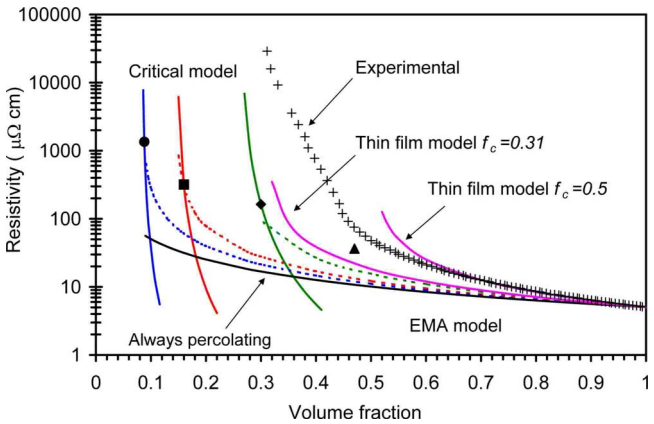


FIG. 8. (Color online) Models of resistivity (dashed curves) using Eq. (5b) assuming $d=1/L$, with $L$ values from Table II based on optical data for the three samples with $f<0.5$. The experimental points are also plotted for these and the $f=0.47$ sample, along with those for growing gold films (x). Symmetric model curves (solid) are also plotted for $f_c=0.31$ as found for normal gold films, for $f_c=0.50$ as expected from basic morphology, and for $f_c=0$. For interest critical behavior for a single high hyperdimension is plotted for the three low $f$ samples using Eq. (1) and a common $\alpha=2.7$.

rameters pass remarkably close to the actual data points for the two lowest $f$ values.

Whether these model plots remain hypothetical and porous gold is always restrained to evolve at low $f$ along the curve of Fig. 7 remains to be seen. However since departures from this curve are seen in normal gold films as $f$ approaches $f_c$ we cannot yet rule them out. The driving force of structural stability may allow for other stable structural evolution. As seen here, high hyperdimensional behavior can be seen as a consequence of a more branching network and higher average coordination number $z$ evolving as $f$ falls, to avoid structural collapse.

While hyperdimensionality can be considered in terms of the parameter $d=z/2$ in Eq. (5) it may not be practical to justify it using critical plots as in Fig. 3 to find $\alpha$. However, assuming a high $d$ value, it seems that a value of $\alpha$ at or below 2, as needed for three dimensions, is unlikely to work on the samples with very low $f$. This adds weight to the case for hyperdimensionality while the observed departure of the normal gold films from a $d=2$ critical response is clearly nonuniversal. Various other explanations proposed for departure from universality do not seem to work here, apart from explaining small down-shifts such as from $d=3.0$ to 2.8. This data thus points to a need either for some new explanations of departures from universality or its reappraisal in terms of $d$ rather than the applicable $D$.

## VI. CONCLUSION

Nanoporous gold in complex three-dimensional networks can percolate at very low volume fill factors $f$ of gold. As $f$ falls, models of optical and resistivity data provide evidence that morphology seems to evolve continuously for $f$ values less than 0.5 as the mobile gold atoms move during etching to ensure structural stability. Final structures seem to have a common underlying symmetry as seen in universal fractal-like behavior found for resistivity from $f=1.0$ to $f=0.08$ consistent with gold networks growing by diffusion-limited aggregation. Greater branching and an associated varying hyperdimensional character emerges as $f$ drops. Normal thin films of gold on glass depart from this universal plot via changes in structural evolution once $f<0.65$ to yield an anomalous critical threshold and nonuniversal coefficients. The issue of universality needs reexamining in the light of this data, while further experiments on gold and other nanoporous metals are needed to better understand these unusual results, to assess if the low $f$ samples are optically anisotropic, to explore if alternative optical effective models to that of Bruggeman designed for near critical behavior[17–19] are applicable and to see if gold's ability to adjust structurally to yield percolating structures with such low metal content is unique. A simple approach to extracting critical coefficients from optical data has been suggested based on effective plasmonic response near the critical threshold.

## ACKNOWLEDGMENTS

We thank Angus Gentle for help with interpreting optical data and Ric Wuhrer for help with imaging.

[1] K. Seal, M. A. Nelson, Z. Charles, D. A. Genov, A. K. Sarychev, and V. M. Shalaev, J. Mod. Opt. **49**, 2423 (2002).
[2] G. B. Smith, G. A. Niklasson, J. S. E. M. Svensson, and C. G. Granqvist, J. Appl. Phys. **59**, 571 (1986).
[3] S. Xu, B. L. Evans, D. I. Flynn, and C. En, Thin Solid Films **238**, 54 (1994).
[4] Y. Yagil, P. Gadenne, C. Julien, and G. Deutscher, Phys. Rev. B **46**, 2503 (1992).
[5] A. I. Maaroof and B. L. Evans, J. Appl. Phys. **76**, 1047 (1994).
[6] S. O. Kucheyev, J. R. Hayes, J. Biener, T. Huser, B. C. E. Talley, and A. V. Hamza, Appl. Phys. Lett. **89**, 053102 (2006).
[7] L. H. Qian, X. Q. Yan, T. Fujita, A. Inoue, and M. W. Chen, Appl. Phys. Lett. **90**, 153120 (2007).
[8] G. B. Smith A. R. Gentle, and A. I. Maaroof, J. Nanophotonics **1**, 013507 (2007).
[9] A. I. Maaroof, A. Gentle, G. B. Smith, and M. B. Cortie, J. Phys. D **40**, 5675 (2007).
[10] A. I. Maaroof, M. B. Cortie, and G. B. Smith, J. Opt. A, Pure Appl. Opt. **7**, 303 (2005).
[11] A. Mortari, A. I. Maaroof, D. Martin, and M. B. Cortie, Sens. Actuators B **123**, 262 (2007).
[12] M. B. Cortie, A. I. Maaroof, and G. B. Smith, Gold Bull. **38**, 15 (2005).
[13] L. Glaner, E. Van der Lingen, and M. B. Cortie, Australian Patent No. 2,150,39 (30 January 2003).
[14] C. Xu, J. Su, X. Xu, P. Liu, H. Zhao, F. Tian, and Y. Ding, J. Am. Chem. Soc. **129**, 42 (2007).
[15] D. Stauffer and A. Aharony, *Introduction to Percolation Theory*, 2nd ed. (Taylor & Francis, London, 1992).
[16] P. M. Chaikin and T. C. Lubensky, *Principles of Condensed Matter Physics* (Cambridge University Press, Cambridge, UK, 1995), p. 230.
[17] J. Wu and D. S. McLachlan, Phys. Rev. B **56**, 1236 (1997).
[18] C. Chiteme and D. S. McLachlan, Phys. Rev. B **67**, 024206 (2003).
[19] W. Z. Cai, S. T. Tu, and J. M. Gong, J. Compos. Mater. **40**, 2131 (2006).
[20] J. N. Roberts and L. M. Schwartz, Phys. Rev. B **31**, 5990 (1985).
[21] S. Shabtaie and C. R. Bentley, J. Geophys. Res. **99**, 19,757 (1994).
[22] G. B. Smith, G. A. Niklasson, J. S. E. M. Svensson, and C. G. Granqvist, Sol. Energy Mater. **14**, 257 (1986).
[23] G. A. Niklasson and C. G. Granqvist, J. Appl. Phys. **55**, 3382 (1984).
[24] J. S. Helman and B. Abeles, Phys. Rev. Lett. **37**, 1429 (1976).
[25] S. Grésillon, L. Aigouy, A. C. Boccara, J. C. Rivoal, X. Quelin, C. Desmarest, P. Gadenne, V. A. Shubin, A. K. Sarychev, and V. M. Shalaev, Phys. Rev. Lett. **82**, 4520 (1999).
[26] K. Seal, A. K. Sarychev, H. Noh, D. A. Genov, A. Yamilov, V. M. Shalaev, Z. C. Ying, and H. Cao, Phys. Rev. Lett. **94**,

226101 (2005).
[27] B. I. Halperin, S. Feng, and P. N. Sen, Phys. Rev. Lett. **54**, 2391 (1985).
[28] S. Feng, B. I. Halperin, and P. N. Sen, Phys. Rev. B **35**, 197 (1987).
[29] I. Balberg, Philos. Mag. B **56**, 991 (1987).
[30] R. W. Cohen, C. G. Cody, M. D. Coutts, and B. Abeles, Phys. Rev. B **8**, 3689 (1973).
[31] G. B. Smith, A. Maaroof, and A. Gentle, Opt. Commun. **271**, 263 (2007).
[32] A. I. Maaroof, A. R. Gentle, M. B. Cortie, and G. B. Smith, Proc. SPIE **6647**, 6647OD1 (2007).
[33] D. A. G. Bruggeman, Ann. Phys. **416**, 636 (1935).
[34] G. B. Smith, J. Phys. D **10**, L39 (1977).
[35] G. B. Smith, Appl. Phys. Lett. **35**, 668 (1979).
[36] G. B. Smith, G. A. Niklasson, J. S. E. M. Svensson, and C. G. Granqvist, Proc. SPIE **562**, 116 (1985).
[37] B. T. Draine and P. J. Flatau, J. Opt. Soc. Am. A **11**, 1491 (1994).
[38] M. I. Mishchenko, J. W. Hovenier, and L. D. Travis, *Light Scattering by Nonspherical Particles: Theory, Measurements, and Geophysical Applications* (Academic, New York, 2000), pp. 131–145.
[39] W. Xia and M. F. Thorpe, Phys. Rev. A **38**, 2650 (1988).
[40] D. S. McLachlan, J. Phys. C **20**, 865 (1987).
[41] J. P. Clerc, G. Giraud, J. M. Laugier, and J. M. Luck, Adv. Phys. **39**, 191 (1990).
[42] X. Zhang and D. Stroud, Phys. Rev. B **52**, 2131 (1995).
[43] B. Abeles, H. L. Pinch, and J. I. Gittleman, Phys. Rev. Lett. **35**, 247 (1975).